ChemPubSoc Europe

DOI: 10.1002/chem.201404349

CHEMISTRY
A European Journal
Communication

Metal–Oxo Reactivity

Dramatic Influence of an Anionic Donor on the Oxygen-Atom Transfer Reactivity of a Mn^{V}–Oxo Complex

Heather M. Neu,[a] Matthew G. Quesne,[b] Tzuhsiung Yang,[a] Katharine A. Prokop-Prigge,[a] Kyle M. Lancaster,[c] James Donohoe,[c] Serena DeBeer,*[c, d] Sam P. de Visser,*[b] and David P. Goldberg*[a]

Abstract: Addition of an anionic donor to an $Mn^{V}(O)$ porphyrinoid complex causes a dramatic increase in 2-electron oxygen-atom-transfer (OAT) chemistry. The 6-coordinate $[Mn^{V}(O)(TBP_8Cz)(CN)]^-$ was generated from addition of $Bu_4N^+CN^-$ to the 5-coordinate $Mn^{V}(O)$ precursor. The cyanide-ligated complex was characterized for the first time by Mn K-edge X-ray absorption spectroscopy (XAS) and gives Mn–O = 1.53 Å, Mn–CN = 2.21 Å. In combination with computational studies these distances were shown to correlate with a singlet ground state. Reaction of the CN^- complex with thioethers results in OAT to give the corresponding sulfoxide and a $2e^-$-reduced $Mn^{III}(CN)^-$ complex. Kinetic measurements reveal a dramatic rate enhancement for OAT of approximately 24000-fold versus the same reaction for the parent 5-coordinate complex. An Eyring analysis gives $\Delta H^{\neq} = 14\ kcal\,mol^{-1}$, $\Delta S^{\neq} = -10\ cal\,mol^{-1}\,K^{-1}$. Computational studies fully support the structures, spin states, and relative reactivity of the 5- and 6-coordinate $Mn^{V}(O)$ complexes.

Determining the factors that control the inherent reactivity of metal–oxo complexes is of critical importance for understanding the function of both heme and nonheme metalloenzymes. Heme enzymes can be differentiated by the protein-derived axial ligand which binds the heme cofactor through one of the axial positions of the central metal ion. For example, peroxidases employ a histidine,[1] catalases employ a tyrosinate,[2] and Cytochrome P450s (CYP450) utilize a cysteinate ligand to coordinate to the iron center.[3] It has been suggested that the anionic Cys donor in CYP450 plays an important role in modulating the electronic features and reactivity of the high-valent iron–oxo species $Fe^{IV}(O)(porph^{+\bullet})(Cys)$ (Compound-I: Cpd-I), which is the critical intermediate responsible for substrate oxidation.[3]

The influence of axial ligands on the reactivity of synthetic Cpd-I analogues has been examined for several reaction classes, including alkyl and arene hydroxylation, and alkene epoxidation.[4] These previous studies have shown that both anionic and neutral donors have had a significant influence on the reactivity of the Cpd-I analogues, with reaction rates typically being influenced by 1–3 orders of magnitude. However, the fundamental origins of these axial ligand effects are still not well understood, and some of the explanations that were offered provide conflicting conclusions. The analogous influence of axial ligands on high-valent Mn–oxo complexes has been less well studied, in part because Cpd-I analogues $Mn^{IV}(O)(porph^{+\bullet})$, or the equivalent $Mn^{V}(O)(porph^{0})$, are typically highly unstable and difficult to observe.[5,6] We previously examined axial ligand effects on a high-valent manganese(V)–oxo complex, $Mn^{V}(O)(TBP_8Cz)$, [TBP_8Cz = octakis(*p-tert*-butylphenyl)corrolazinato^{3-}], which is a rare example of a stable and isolable $Mn^{V}(O)$ porphyrinoid species.[7,8] Reactivity towards C–H substrates was examined, and dramatic increases in hydrogen-atom transfer (HAT) rates were observed upon addition of anionic donors (e.g., F^-, CN^-). It was concluded that the anionic donors were weakly coordinating *trans* to the oxo ligand, and based on density functional theory (DFT) calculations, the axial ligands likely caused an increase in the basicity of the incipient $[Mn^{IV}(OH)]^-$ intermediate and a strengthening of the O–H bond. This thermodynamic influence, in turn, led to a greater overall driving force for HAT, which correlated with a lowering of the reaction barrier.[8a] An alternative explanation for the HAT reactivity based on additional DFT calculations was recently offered, and involves spin cross-over from the low-spin (ls) singlet ($S = 0$) state for $[Mn^{V}(O)(TBP_8Cz)(CN)]^-$ to a high-spin (hs) triplet ($S = 1$) state.[9]

In this work we provide novel insights regarding the axial ligand effects on the OAT reactivity of a high-valent $Mn^{V}(O)$

[a] *H. M. Neu, T. Yang, Dr. K. A. Prokop-Prigge, Prof. D. P. Goldberg*
Department of Chemistry, The Johns Hopkins University
Baltimore, MD (USA)
E-mail: dpg@jhu.edu

[b] *Dr. M. G. Quesne, Dr. S. P. de Visser*
Manchester Institute of Biotechnology and
School of Chemical Engineering and Analytical Science
The University of Manchester, 131 Princess Street, Manchester (UK)
E-mail: sam.devisser@manchester.ac.uk

[c] *Prof. K. M. Lancaster, J. Donohoe, Prof. S. DeBeer*
Department of Chemistry and Chemical Biology, Cornell University
Ithaca, New York (USA)

[d] *Prof. S. DeBeer*
Max-Planck Institute for Chemical Energy Conversion, Stiftstrasse
Mülheim an der Ruhr (Germany)
E-mail: serena.debeer@cec.mpg.de

Supporting information for this article is available on the WWW under http://dx.doi.org/10.1002/chem.201404349.

complex. Addition of the mono-anionic donor CN^- leads to the formation of the 6-coordinate complex $[Mn^V(O)(TBP_8Cz)(CN)]^-$. X-ray absorption spectroscopy (XAS) measurements provided structural parameters and an oxidation state assignment for this complex. The oxygen-atom-transfer (OAT) reactivity of this complex was examined for thioether substrates, and a dramatic rate acceleration of approximately 24000-fold over the 5-coordinate parent complex was observed. This increase in reactivity is orders of magnitude larger than that seen in similar studies on the axial ligand influence in either heme- or nonheme high-valent metal–oxo complexes of biological relevance.[4,5,10] Computational (DFT) methods led to optimized geometries that were in good agreement with the XAS studies, and these experimentally validated computational results help shed light on the ground spin states for the $Mn^V(O)$ complexes. Further DFT calculations on the OAT reaction profiles fully support the experimentally observed increase in reaction rate.

In an earlier study we showed that addition of excess $Bu_4N^+CN^-$ to $Mn^V(O)(TBP_8Cz)$ in CH_2Cl_2 led to a large increase in HAT reactivity.[8a] The UV/Vis spectrum of the $Mn^V(O)$ complex is not sensitive to addition of CN^-, but LDI-MS (neg. mode) showed clear evidence for a complex matching the formula $[Mn^V(O)(TBP_8Cz)(CN)]^-$, consistent with formation of a 6-coordinate complex as seen in Scheme 1. However, direct structural information on the cyanide-ligated complex was lacking, in part due to the instability of this complex. We now report the structural characterization of $[Mn^V(O)(TBP_8Cz)(CN)]^-$ by XAS. The Mn K-edge XAS spectra of $Mn^V(O)(TBP_8Cz)$ and $[Mn^V(O)(TBP_8Cz)(CN)]^-$ (prepared by addition of 10 and 100 equivalents of $Bu_4N^+CN^-$) are shown in Figure 1a. All three spectra are consistent with a Mn^V oxidation state assignment, based on the approximately 6553 eV position of the rising edge. Upon addition of CN^-, the edge shifts by about 0.3 eV to lower energy, but not enough to suggest reduction to Mn^{IV}. Most notably, upon addition of CN^-, the pre-edge remains at high energy (~6542 eV), but the pre-edge intensity decreases relative to the 5-coordinate Mn^V–oxo complex. These data are consistent with formation of a 6-coordinate Mn^V–oxo species. Coordination of a *trans* axial CN^- ligand would move the Mn further into the Cz plane, decreasing the amount of metal 3d–4p mixing, and thus decreasing the observed pre-edge intensity.

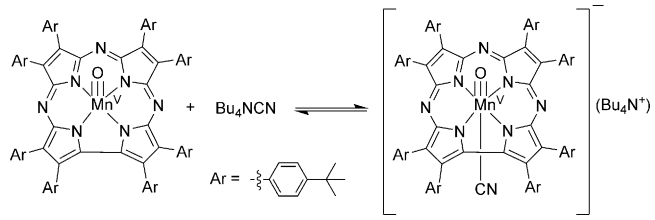

Scheme 1. Formation of 6-coordinate $[Mn^V(O)(TBP_8Cz)(CN)]^-$.

Figure 1b shows the EXAFS data for $Mn^V(O)(TBP_8Cz)$ and $[Mn^V(O)(TBP_8Cz)(CN)]^-$ (at 100-fold excess of $Bu_4N^+CN^-$) with the corresponding Fourier transforms (FTs) presented in Figure 1c. These data clearly show that addition of CN^- introduces a structural perturbation at the Mn site. The overall beat pattern of the EXAFS is altered and the relative intensity of the FT peaks is also modified. Based on our EXAFS fits, these trends are best interpreted as resulting from direct coordination of CN^- to $Mn^V(O)(TBP_8Cz)$. The 5-coordinate $Mn^V(O)(TBP_8Cz)$ is best fit by inclusion of one Mn–O vector at 1.54 Å and 4 Mn–N(Cz) interactions at 1.87 Å, and multiple scattering (MS) interactions from the Cz ring are needed to fit the outer-shell contributions to the FT (see the Supporting Information for full fit parameters). These data match well with an earlier report, and were repeated here for the direct comparison with $[Mn^V(O)(TBP_8Cz)(CN)]^-$.[8b] For $[Mn^V(O)(TBP_8Cz)(CN)]^-$, the data are best fit by one Mn–O at 1.53 Å, four Mn–N(Cz) interactions at 1.87 Å, and a 2.21 Å Mn–C/N interaction consistent with a coordinated CN^-. The coordination of CN^- is further supported by the increase in the outer-shell FT amplitude (despite the decrease in the first shell amplitude). The increase in outer-shell multiple scattering intensity at approximately 2.5 Å is attributed to the presence of linear scattering from the nitrogen of coordinated CN^-, in addition to Cz ring scattering.

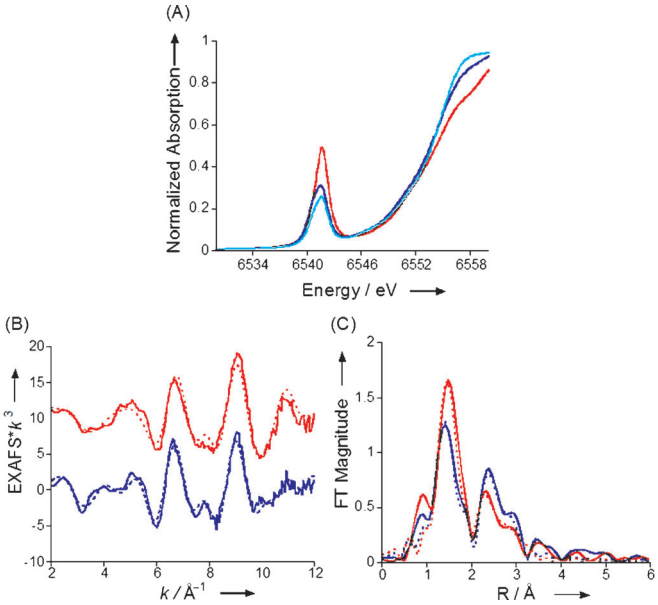

Figure 1. A) Comparison of the normalized Mn K-edge XAS data for $Mn^V(O)(TBP_8Cz)$ with zero (red), 10 (dark blue) and 100 (light blue) equivalents of added $Bu_4N^+CN^-$ in benzonitrile. B) EXAFS data (solid lines) and fits (dashed lines) for $Mn^V(O)(TBP_8Cz)$ (red) and $Mn^V(O)(TBP_8Cz)+100$ equivalents of $Bu_4N^+CN^-$ (blue). C) The corresponding FTs (solid) and fits (dashed).

Reactivity studies with the cyanide complex $[Mn^V(O)(TBP_8Cz)(CN)]^-$ were undertaken to determine the influence of anionic axial donors on OAT reactivity. This species was allowed to react with dibutyl sulfide (DBS) in toluene at 25 °C (Scheme 2). This reaction was monitored by UV/Vis spectroscopy as shown in Figure 2, and exhibited rapid isosbestic conversion of $[Mn^V(O)(TBP_8Cz)(CN)]^-$ to a species with a split Soret band at 443 and 492 nm, and a Q-band at 694 nm. This final spectrum can be assigned to the $2e^-$-reduced Mn^{III} complex $[Mn^{III}(TBP_8Cz)(CN)]^-$, as confirmed by independent generation. The related chloride-ligated complex $(Et_4N)[Mn^{III}(TBP_8Cz)(Cl)]$ also exhibits a similar split Soret band and has been crystallo-

graphically characterized.[8b,c] The reaction was complete within a few minutes, as compared to several hours for the reaction of the 5-coordinate $Mn^{V}(O)$ complex with the same substrate at much larger concentrations.[8d] These data clearly demonstrate that addition of CN^{-} leads to a large increase in reactivity towards DBS.

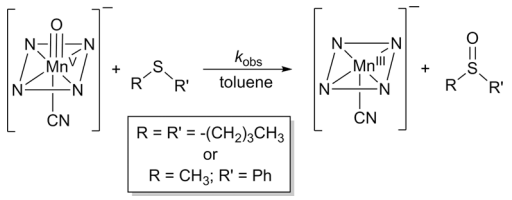

Scheme 2. Reaction of $[Mn^{V}(O)(TBP_8Cz)(CN)]^{-}$ with thioether substrates.

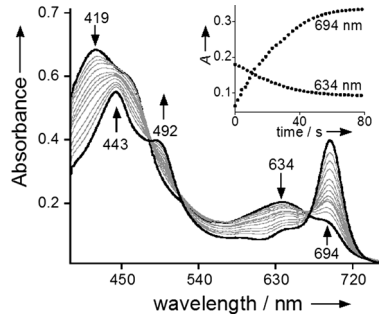

Figure 2. UV/Vis spectral changes (0–80 s) for the reaction of $[Mn^{V}(O)(TBP_8Cz)(CN)]^{-}$ (11 μM) (419, 634 nm) with excess DBS (500 equiv) to give $[Mn^{III}(TBP_8Cz)(CN)]^{-}$ (443, 492, 694 nm) in toluene at 25 °C. Inset: changes in absorbance versus time for the growth of $[Mn^{III}(TBP_8Cz)(CN)]^{-}$ (694 nm) and the decay of $[Mn^{V}(O)(TBP_8Cz)(CN)]^{-}$ (634 nm).

A second substrate, thioanisole (PhSMe), was tested to examine the generality of the CN^{-} influence over OAT reactivity with thioethers, and provides a convenient substrate for measuring quantitative yields of sulfoxide product by GC-FID. The reaction between PhSMe and $[Mn^{V}(O)(TBP_8Cz)(CN)]^{-}$ led to the expected conversion of the starting material to the cyanide-ligated Mn^{III} product, and the reaction mixture was analyzed directly by GC-FID. The anticipated methyl phenyl sulfoxide was obtained in high yield (84%; Scheme 2). Labeling of the terminal oxo ligand with ^{18}O from $H_2{}^{18}O$, followed by reaction with PhSMe led to 71% incorporation of ^{18}O in the final sulfoxide product as seen by GC-MS. These data show that $[Mn^{V}(O)(TBP_8Cz)(CN)]^{-}$ carries out direct OAT to thioethers to give the $2e^{-}$-oxidized sulfoxide as the major product.

The kinetics of OAT for $[Mn^{V}(O)(TBP_8Cz)(CN)]^{-}$ with DBS as substrate were quantitatively analyzed for comparison with the previously examined 5-coordinate $Mn^{V}(O)$ complex (second-order rate constant of $3.8\times10^{-4}\,M^{-1}s^{-1}$ for DBS).[8d] Reactions were run under pseudo-first-order conditions (175–750 equiv of DBS) and monitored by UV/Vis. Isosbestic behavior was observed as seen in Figure 2 for all concentrations of DBS, and plots of absorbance versus time for the decay of the $[Mn^{V}(O)(TBP_8Cz)(CN)]^{-}$ complex (634 nm) and the appearance of the $[Mn^{III}(TBP_8Cz)(CN)]^{-}$ complex (694 nm) were well-fit by a single exponential model. The resulting fits yielded the pseudo-first-order rate constants k_{obs}, and plots of k_{obs} at 694 or 634 nm versus [DBS] were linear. The kinetics are consistent with the overall second-order rate law: $-d[Mn^{V}(O)(X)]/dt = k[Mn^{V}(O)(X)][DBS]$, and the slope of the best-fit line of the second-order plot for 694 nm gives $k = 9.2(\pm0.3)\,M^{-1}s^{-1}$. A comparison of the rate constant for the CN^{-} complex with that reported for the 5-coordinate $Mn^{V}(O)$ complex reveals a dramatic rate enhancement of 24000-fold for OAT with DBS as substrate. This change can be compared to recent work by Fujii, which showed that modifying the nature of the axial ligand in an iron–oxo porphyrin Cpd-I analogue resulted in a 30-fold difference in OAT rate.[4a]

To obtain further information on the mechanism of OAT for $[Mn^{V}(O)(TBP_8Cz)(CN)]^{-}$ and DBS, a temperature-dependent study of the rate constants (−20 to 40 °C) was performed. An Eyring plot of $\ln(k/T)$ versus $1/T$ (Figure 3) shows a linear dependence that yields the activation parameters listed in Table 1. The activation parameters for the 5-coordinate $Mn^{V}(O)$ complex, and the one-electron-oxidized analogue $Mn^{V}(O)(TBP_8Cz^{+\bullet})$, are included in Table 1 for comparison, measured previously for the same substrate and solvent.[8d] The enthalpy of activation for the cyanide-ligated complex is lower than that found for the 5-coordinate complex, while the $\Delta S^{\neq}$ is more positive. These differences both contribute to a lowering of the reaction barrier for the CN^{-} complex. The overall negative $\Delta S^{\neq}$ value for the CN^{-} complex is consistent with a bimolecular mechanism, while the unusually large and negative $\Delta S^{\neq}$ seen for the positively charged $Mn^{V}(O)(TBP_8Cz^{+\bullet})$ is not observed for the negatively charged CN^{-} complex. From these data, it appears that the addition of CN^{-} to the $Mn^{V}(O)$ complex does not cause a significant change in the mechanism of OAT, but does induce a significant lowering of the reaction barrier through a combination of both enthalpic and entropic effects.

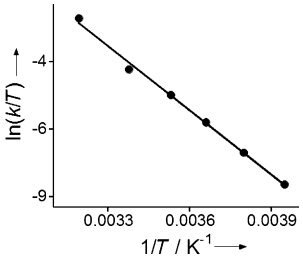

Figure 3. Eyring plot for the reaction of $[Mn^{V}(O)(TBP_8Cz)(CN)]^{-}$ (11.5 μM) with DBS (21 mM) in toluene from −20 to 40 °C.

Table 1. Kinetic and activation parameters for OAT reactions with dibutyl sulfide.

	$Mn^{V}(O)(TBP_8Cz)$[a]	$Mn^{V}(O)(TBP_8Cz^{+\bullet})$[a]	$[Mn^{V}(O)(TBP_8Cz)(CN)]^{-}$
k[b]	3.8×10^{-4}[c]	$(6.2\pm0.2)\times10^{-3}$	9.2 ± 0.3
$\Delta H^{\neq}$[d]	16 ± 1	7.0 ± 0.8	14 ± 0.4
$\Delta S^{\neq}$[e]	-20 ± 4	-45 ± 3	-10 ± 0.8
$\Delta G^{\neq}$[d]	22 ± 2[f]	20 ± 2[f]	17 ± 0.5[f]

[a] From Ref. [8d]. [b] Values in $M^{-1}s^{-1}$ at 298 K. [c] Extrapolated from a $\ln(k/T)$ versus $1/T$ plot. [d] Values in kcal mol^{-1}. [e] Values in cal K^{-1} mol^{-1}. [f] At 298 K.

Computational studies were employed to gain further insight into the structure and reactivity of $[Mn^{V}(O)(TBP_8Cz)(CN)]^-$. Previous calculations on the 5- and 6-coordinate $Mn^{V}(O)$ complexes[8d] utilized an abbreviated Cz core with hydrogen atoms on all β-carbon positions (H_8Cz) for computational convenience. To determine the influence of the peripheral substituents on the computational results, a set of DFT calculations with H_8Cz, octamethyl (Me_8Cz), and octamethylphenyl ($(MePh)_8Cz$) corrolazine ligands were performed for both the $Mn^{V}(O)$ and $[Mn^{V}(O)(CN)]^-$ complexes. Three different density functional methods were also employed for all complexes, providing a comprehensive DFT analysis of optimized geometries and spin ground states.[11] Although a certain degree of fluctuation in spin state ordering and relative energies is obtained between the different DFT methods, the majority of calculations give a singlet spin ground state. The Mn–O bond is shortest in the closed-shell singlet spin ground state; with Mn–O = 1.55 Å at B3LYP-D3/SDD/6-31G(d) level of theory, as expected for a low-spin d^2 ion with both π*(MnO) orbitals unoccupied. The excited triplet spin states for the $[Mn^{V}(O)(CN)]^-$ complexes exhibit different electronic configurations depending upon which functional is employed. For B3LYP and M06, spin densities indicate an electronic configuration that can be best described as a hs-Mn^{IV}(oxyl radical), whereas BP86 results in a configuration closer to a hs-Mn^{V} ($d^1\pi^{*1}$ state). The oxyl radical states give highly elongated Mn–O bonds (1.80–1.82 Å), and although the hs-Mn^{V} state has a shorter distance of approximately 1.67 Å, all of these Mn–O distances are significantly longer than that observed by EXAFS. Thus the DFT-optimized geometries for the singlet spin states provide the best match for the structure obtained by EXAFS. Time-dependent DFT calculations on the singlet states for the 5- and 6-coordinate complexes also reproduce the qualitative trend in the lowering of the pre-edge peak intensity for the CN^- complex. From our combined spectroscopic and computational studies, we conclude that $[Mn^{V}(O)(TBP_8Cz)(CN)]^-$ has a low-spin singlet ground state. This state is the same as that seen for the five-coordinate $Mn^{V}(O)$ complex, and these data indicate that CN^- ligation does not perturb the spin ground state.

To further establish the electronic ground state and orbital occupations of the lowest energy singlet and triplet spin states of $[Mn^{V}(O)(H_8Cz)(CN)]^-$ we ran a series of CASSCF-NEVPT2 calculations on the B3LYP optimized geometries. We find a singlet spin ground state with the triplet higher in energy by 13 kcal mol^{-1}. This singlet–triplet energy gap is considerably larger than that found from DFT, and indicates that reactivity on the triplet spin state surface is highly unlikely. Interestingly, the NEVPT2 calculated triplet spin state gives spin densities of 2.1 on Mn and −0.1 on O, whereas the DFT result gives spin densities of about 3 on Mn and −1 on O instead. These results implicate that the DFT calculated triplet spin state may be a spurious artefact that has no realistic electronic structure. Further studies are needed to establish the exact nature of the triplet spin state and its reactivity, and therefore we will focus on the singlet spin state only.

To gain insight into the mechanism of OAT, we then did a set of DFT studies on dimethyl sulfide sulfoxidation by $[Mn^{V}(O)(H_8Cz)(L)]$ with L = no ligand (NL) or CN^-. Figure 4 shows the potential energy profile and rate determining transition state geometries for the sulfoxidation reaction. Similar to previous studies, sulfoxidation is a concerted reaction process with a single S–O bond formation transition state, $\mathbf{TS}_L$.[8d,12] The enthalpy of activation (with solvent corrections included) is lowered dramatically upon addition of an axial ligand, in good agreement with the large rate enhancement observed for the 6-coordinate complex. A close inspection of the transition state geometries reveals that $^1\mathbf{TS}_{SO,CN}$ is earlier on the potential energy surface than $^1\mathbf{TS}_{SO,NL}$ with a longer S–O distance and shorter Mn–O distance. Often early transition states correspond to lower energetic barriers than late transition states.[13] The lowering of the barrier may also be related to the stabilization of the Mn^{III} product via coordination of CN^-. This computational result is in agreement with Fujii's recent analysis that the increase in oxidative reactivity of Cpd-I analogues with different axial ligands can be ascribed to the energetics of axial ligand stabilization of the Fe^{III}(porph) products.[4] Future experimental and computational work is warranted to determine the origins of the lowering of the reaction barrier in Figure 4.

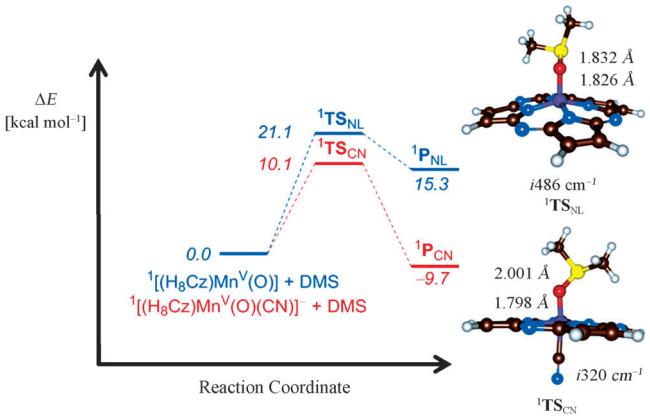

Figure 4. Potential energy profile calculated at UB3LYP/BS2 level of theory for OAT reactions involving $[Mn^{V}(O)(H_8Cz)]$ and $[Mn^{V}(O)(H_8Cz)(CN)]^-$ with DMS. Energies ($\Delta E + ZPE + E_{solv}$) are given. Also shown are optimized transition state geometries (right-hand side) with bond lengths in angstroms and the imaginary mode in wave numbers.

Our combined experimental and computational studies demonstrate that the addition of an anionic axial ligand to an $Mn^{V}(O)$ porphyrinoid complex results in a remarkable increase in OAT reaction rate with thioether substrates. The XAS data and DFT calculations indicate that the singlet ground state, and associated short Mn–O distance, for the 5-coordinate $Mn^{V}(O)$ complex does not change upon addition of an anionic axial ligand. The OAT mechanism appears to be a concerted $2e^-$ process, leading to the smooth formation of $[Mn^{III}(CN)]^-$ and sulfoxide products. The DFT studies reproduce well the observed increase in reaction rate by a significant stabilization of the reaction barrier for the $^1[Mn^{V}(O)(TBP_8Cz)(CN)]^-$ complex. Future studies will be aimed at determining the generality of the axial ligand effects on OAT reactivity for $Mn^{V}(O)$ complexes.

Acknowledgements

This work was supported by the NSF (CHE0909587 and CHE121386 to D.P.G.) and the NIH (GM101153 to D.P.G). BBSRC is acknowledged for a studentship to M.G.Q. and the National Service of Computational Chemistry Software (NSCCS) is thanked for cpu time to S.d.V. Portions of this research were carried out at SSRL, a national user facility operated by Stanford University on behalf of the US DOE, BES. We thank Prof. K. D. Karlin for instrumentation use. The Kirin cluster at Johns Hopkins University School of Arts and Sciences is thanked for cpu time to T.Y.

Keywords: manganese · oxygen-atom-transfer · porphyrinoids · spin state reactivity · sulfoxidation

[1] a) G. Battistuzzi, M. Bellei, C. A. Bortolotti, M. Sola, *Arch. Biochem. Biophys.* **2010**, *500*, 21 – 36; b) T. L. Poulos, in *Handbook of Porphyrin Science* Vol. 19 (Eds.: K. M. Kadish, K. M. Smith, R. Guilard), World Scientific Publishing, Singapore, **2012**, pp. 45 – 109; c) K. D. Bewley, K. E. Ellis, M. A. Firer-Sherwood, S. J. Elliott, *Biochim. Biophys. Acta Bioenerg.* **2013**, *1827*, 938 – 948.

[2] a) A. Díaz, P. C. Loewen, I. Fita, X. Carpena, *Arch. Biochem. Biophys.* **2012**, *525*, 102 – 110; b) M. Alfonso-Prieto, P. Vidossich, C. Rovira, *Arch. Biochem. Biophys.* **2012**, *525*, 121 – 130.

[3] a) J. T. Groves, *Nat. Chem.* **2014**, *6*, 89 – 91; b) M. T. Green, *Curr. Opin. Chem. Biol.* **2009**, *13*, 84 – 88; c) M. T. Green, J. H. Dawson, H. B. Gray, *Science* **2004**, *304*, 1653 – 1656; d) T. H. Yosca, J. Rittle, C. M. Krest, E. L. Onderko, A. Silakov, J. C. Calixto, R. K. Behan, M. T. Green, *Science* **2013**, *342*, 825 – 829; e) T. L. Poulos, B. C. Finzel, A. J. Howard, *J. Mol. Biol.* **1987**, *195*, 687 – 700; f) I. G. Denisov, T. M. Makris, S. G. Sligar, I. Schlichting, *Chem. Rev.* **2005**, *105*, 2253 – 2277.

[4] a) A. Takahashi, D. Yamaki, K. Ikemura, T. Kurahashi, T. Ogura, M. Hada, H. Fujii, *Inorg. Chem.* **2012**, *51*, 7296 – 7305; b) Z. Gross, *J. Biol. Inorg. Chem.* **1996**, *1*, 368 – 371; c) Y. Kang, H. Chen, Y. J. Jeong, W. Lai, E. H. Bae, S. Shaik, W. Nam, *Chem. Eur. J.* **2009**, *15*, 10039 – 10046; d) A. Takahashi, T. Kurahashi, H. Fujii, *Inorg. Chem.* **2009**, *48*, 2614 – 2625; e) W. J. Song, Y. O. Ryu, R. Song, W. Nam, *J. Biol. Inorg. Chem.* **2005**, *10*, 294 – 304; f) T. Kamachi, T. Kouno, W. Nam, K. Yoshizawa, *J. Inorg. Biochem.* **2006**, *100*, 751 – 754; g) Z. Z. Pan, R. Zhang, M. Newcomb, *J. Inorg. Biochem.* **2006**, *100*, 524 – 532; h) N. Hessenauer-Ilicheva, A. Franke, D. Meyer, W. D. Woggon, R. van Eldik, *J. Am. Chem. Soc.* **2007**, *129*, 12473 – 12479; i) N. Hessenauer-Ilicheva, A. Franke, D. Meyer, W. D. Woggon, R. van Eldik, *Chem. Eur. J.* **2009**, *15*, 2941 – 2959.

[5] a) D. Balcells, C. Raynaud, R. H. Crabtree, O. Eisenstein, *Inorg. Chem.* **2008**, *47*, 10090 – 10099; b) N. Jin, D. E. Lahaye, J. T. Groves, *Inorg. Chem.* **2010**, *49*, 11516 – 11524; c) M. E. Crestoni, S. Fornarini, F. Lanucara, *Chem. Eur. J.* **2009**, *15*, 7863 – 7866; d) Z. Solati, M. Hashemi, S. Hashemnia, E. Shahsevani, Z. Karmand, *J. Mol. Catal. A: Chem.* **2013**, *374*, 27 – 31; e) N. Jin, M. Ibrahim, T. G. Spiro, J. T. Groves, *J. Am. Chem. Soc.* **2007**, *129*, 12416 – 12417.

[6] a) S. S. Marla, J. Lee, J. T. Groves, *Proc. Natl. Acad. Sci. USA* **1997**, *94*, 14243 – 14248; b) N. Jin, J. T. Groves, *J. Am. Chem. Soc.* **1999**, *121*, 2923 – 2924; c) W. J. Song, M. S. Seo, S. D. George, T. Ohta, R. Song, M. J. Kang, T. Tosha, T. Kitagawa, E. I. Solomon, W. Nam, *J. Am. Chem. Soc.* **2007**, *129*, 1268 – 1277; d) W. Nam, I. Kim, M. H. Lim, H. J. Choi, J. S. Lee, H. G. Jang, *Chem. Eur. J.* **2002**, *8*, 2067 – 2071; e) R. Zhang, J. H. Horner, M. Newcomb, *J. Am. Chem. Soc.* **2005**, *127*, 6573 – 6582.

[7] a) A. Kumar, I. Goldberg, M. Botoshansky, Y. Buchman, Z. Gross, *J. Am. Chem. Soc.* **2010**, *132*, 15233 – 15245; b) H. Y. Liu, T. S. Lai, L. L. Yeung, C. K. Chang, *Org. Lett.* **2003**, *5*, 617 – 620; c) H. Y. Liu, F. Yam, Y. T. Xie, X. Y. Li, C. K. Chang, *J. Am. Chem. Soc.* **2009**, *131*, 12890 – 12891.

[8] a) K. A. Prokop, S. P. de Visser, D. P. Goldberg, *Angew. Chem. Int. Ed.* **2010**, *49*, 5091 – 5095; *Angew. Chem.* **2010**, *122*, 5217 – 5221; b) D. E. Lansky, B. Mandimutsira, B. Ramdhanie, M. Clausen, J. Penner-Hahn, S. A. Zvyagin, J. Telser, J. Krzystek, R. Zhan, Z. Ou, K. M. Kadish, L. Zakharov, A. L. Rheingold, D. P. Goldberg, *Inorg. Chem.* **2005**, *44*, 4485 – 4498; c) D. E. Lansky, A. A. Narducci Sarjeant, D. P. Goldberg, *Angew. Chem. Int. Ed.* **2006**, *45*, 8214 – 8217; *Angew. Chem.* **2006**, *118*, 8394 – 8397; d) K. A. Prokop, H. M. Neu, S. P. de Visser, D. P. Goldberg, *J. Am. Chem. Soc.* **2011**, *133*, 15874 – 15877; e) P. Leeladee, R. A. Baglia, K. A. Prokop, R. Latifi, S. P. de Visser, D. P. Goldberg, *J. Am. Chem. Soc.* **2012**, *134*, 10397 – 10400.

[9] D. Janardanan, D. Usharani, S. Shaik, *Angew. Chem. Int. Ed.* **2012**, *51*, 4421 – 4425; *Angew. Chem.* **2012**, *124*, 4497 – 4501.

[10] C. V. Sastri, J. Lee, K. Oh, Y. J. Lee, J. Lee, T. A. Jackson, K. Ray, H. Hirao, W. Shin, J. A. Halfen, J. Kim, L. Que, Jr., S. Shaik, W. Nam, *Proc. Natl. Acad. Sci. USA* **2007**, *104*, 19181 – 19186.

[11] S. P. de Visser, M. G. Quesne, B. Martin, P. Comba, U. Ryde, *Chem. Commun.* **2014**, *50*, 262 – 282.

[12] D. Kumar, G. N. Sastry, S. P. de Visser, *Chem. Eur. J.* **2011**, *17*, 6196 – 6205.

[13] a) M. G. Evans, M. Polanyi, *Trans. Faraday Soc.* **1936**, *32*, 1333 – 1359; b) D. Kumar, B. Karamzadeh, G. N. Sastry, S. P. de Visser, *J. Am. Chem. Soc.* **2010**, *132*, 7656 – 7667.

Received: July 10, 2014
Published online on September 26, 2014

